SUPERCONDUCTIVITY

Ferromagnetic order beyond the superconducting dome in a cuprate superconductor

Tarapada Sarkar[1], D. S. Wei[2,3], J. Zhang[4], N. R. Poniatowski[1], P. R. Mandal[1], A. Kapitulnik[2,3,5,6], Richard L. Greene[1]*

According to conventional wisdom, the extraordinary properties of the cuprate high-temperature superconductors arise from doping a strongly correlated antiferromagnetic insulator. The highly overdoped cuprates—whose doping lies beyond the dome of superconductivity—are considered to be conventional Fermi liquid metals. We report the emergence of itinerant ferromagnetic order below 4 kelvin for doping beyond the superconducting dome in thin films of electron-doped $La_{2-x}Ce_xCuO_4$ (LCCO). The existence of this ferromagnetic order is evidenced by negative, anisotropic, and hysteretic magnetoresistance, hysteretic magnetization, and the polar Kerr effect, all of which are standard signatures of itinerant ferromagnetism in metals. This surprising result suggests that the overdoped cuprates are strongly influenced by electron correlations.

Underdoped cuprates exhibit many ordered phases, including antiferromagnetism (*1*, *2*), charge order (*3*–*5*), and nematicity (*6*). The relationship of these phases to high-temperature (high-T_c) superconductivity has yet to be determined. Moreover, the nature of the much-studied pseudogap phase in the hole-doped cuprates, which appears to end at a critical doping, remains unresolved (*7*). The seemingly conventional overdoped region of the phase diagram [beyond the pseudogap endpoint in hole-doped materials or beyond the Fermi surface reconstruction (FSR) in electron-doped materials] has been studied less systematically, and its importance to the mechanism of superconductivity has largely been dismissed. However, some studies of this region suggest that the physics is not that of a conventional Fermi liquid. For example, in both hole-doped and electron-doped materials, the low-temperature normal-state transport properties are anomalous (*8*, *9*). An extended range of quantum critical transport appears to exist from the FSR doping to the end of the superconducting dome in all cuprates (*10*–*12*).

Here, we report ferromagnetic order in electron-doped $La_{2-x}Ce_xCuO_4$ (LCCO), which further challenges the conventional picture of overdoped cuprates. Hints of magnetism in overdoped hole-doped cuprates at temperatures below 1 K have been reported previously (*13*), and ferromagnetic fluctuations have been reported at higher temperatures (*14*). We provide comprehensive and robust evidence for static ferromagnetic order in LCCO (see below). The existence of a ferromagnetic phase beyond the end of the superconducting dome that competes with the d-wave superconductivity was hypothesized in (*15*); the fluctuations of this phase were invoked to explain the temperature dependence of the magnetic susceptibility (χ) in overdoped $(Bi, Pb)_2Sr_2CuO_{6+\delta}$. This raises the possibility that ferromagnetism is a universal feature of overdoped cuprate physics. However, obtaining direct evidence of static (or itinerant) ferromagnetic order associated with the CuO_2 planes in any cuprate remains experimentally challenging.

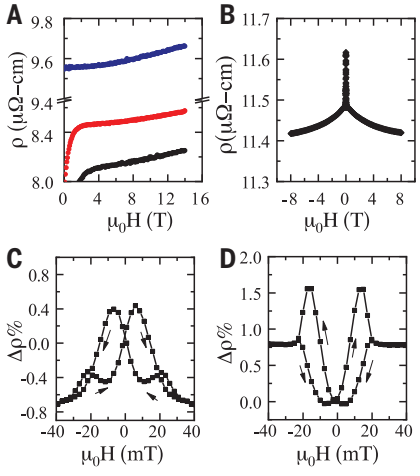

Fig. 1. Low-temperature magnetoresistance across the end of the superconducting dome in LCCO. Shown are the data for a sample on STO substrate. (**A**) *ab*-plane magnetoresistivity ($H \perp ab$-plane) for $x = 0.17$ ($T_c = 4$ K) at 2 K (black), 5 K (red), and 10 K (blue). (**B**) *ab*-plane magnetoresistivity ($H \perp ab$-plane) for $x = 0.18$ at 2 K. (**C** and **D**) *ab*-plane $\Delta\rho(\%) = [\rho(H) - \rho(0)]/\rho(0) \times 100$ for $x = 0.18$ ($T_c = 0$ K) at 2 K in low-field sweep from +400 Oe to −400 Oe for $H \perp ab$-plane (C) and $H \parallel ab$-plane (D). Arrows indicate the sweeping direction of the H field.

To investigate this highly overdoped regime, we measured electron-doped LCCO thin films, which can reliably be doped beyond the superconducting dome. In particular, we focused on the nonsuperconducting dopings ($x = 0.18$, 0.19) where a Fermi liquid–like quadratic temperature dependence of the resistivity is found at low temperatures (*16*).

In Figs. 1 and 2, we present the negative transverse magnetoresistance, anisotropic magnetoresistance, and magnetic field hysteresis in magnetization, magnetoresistance, and magneto-thermopower measurements on LCCO samples grown on $SrTiO_3$ (STO) substrates. Figure 1 shows the low-temperature transverse ($H \perp ab$-plane) magnetoresistance for both a superconducting ($x = 0.17$) and a nonsuperconducting ($x = 0.18$) sample. The magnetoresistance for $x = 0.17$ is positive and crosses over from linear to quadratic in field with increasing temperature, whereas the transverse magnetoresistance for $x = 0.18$ is negative with a strong low-field hysteretic dependence below ~4 K. Both of these features, the negative magnetoresistance and low-field hysteresis below 4 K, are hallmarks of itinerant ferromagnetism (*17*–*20*). Similar magnetoresistance data suggestive of ferromagnetic order are shown in Fig. 2, A and B, for $x = 0.19$, again below 4 K. As shown in Fig. 2D, we also observed hysteresis in the magneto-thermopower (*21*), reaffirming the presence of ferromagnetism and ruling out any current heating effect as the cause of the magnetoresistance hysteresis. In Fig. 2C we show a superconducting quantum interference device (SQUID) magnetization study of a $x = 0.19$ sample, which demonstrates hysteresis in the magnetization below 4 K, with a coercive field comparable to that of the magnetoresistance shown in Fig. 2, A and B. The hysteresis vanishes at 4 K (fig. S1). At 2 K, the magnitude of the magnetization is approximately 0.06 to 0.08 Bohr magneton per formula unit (μ_B/f.u.). The in-plane magnetization saturates, whereas the out-of-plane magnetization does not saturate (Fig. 2C); this shows that the ferromagnetic moments are in the plane, as confirmed by the polar Kerr effect results (Fig. 3) (*22*). Furthermore, we found an anisotropic magnetoresistance, which is a well-known effect intrinsic to ferromagnets, arising from spin-orbit coupling (*17*–*19*). These data are shown in Fig. 1, C and D, and fig. S4, where the magnetoresistance depends on the relative orientation of the current and the magnetization.

In Fig. 3, we show the polar Kerr effect measurements of an $x = 0.19$ LCCO film grown on an $(LaAlO_3)_{0.3}(Sr_2TaAlO_6)_{0.7}$ (LSAT) substrate. For these high-resolution measurements, we used a zero-area loop Sagnac interferometer that nulls out any reciprocal effects such as linear birefringence and is capable of detecting

[1]Maryland Quantum Materials Center and Department of Physics, University of Maryland, College Park, MD 20742, USA. [2]Geballe Laboratory for Advanced Materials, Stanford University, Stanford, CA 94305, USA. [3]Department of Applied Physics, Stanford University, Stanford, CA 94305, USA. [4]State Key Laboratory of Surface Physics, Department of Physics, Fudan University, Shanghai 200433, People's Republic of China. [5]Department of Physics, Stanford University, Stanford, CA 94305, USA. [6]Stanford Institute for Materials and Energy Sciences (SIMES), SLAC National Accelerator Laboratory, Menlo Park, CA 94025, USA.
*Corresponding author. Email: rickg@umd.edu

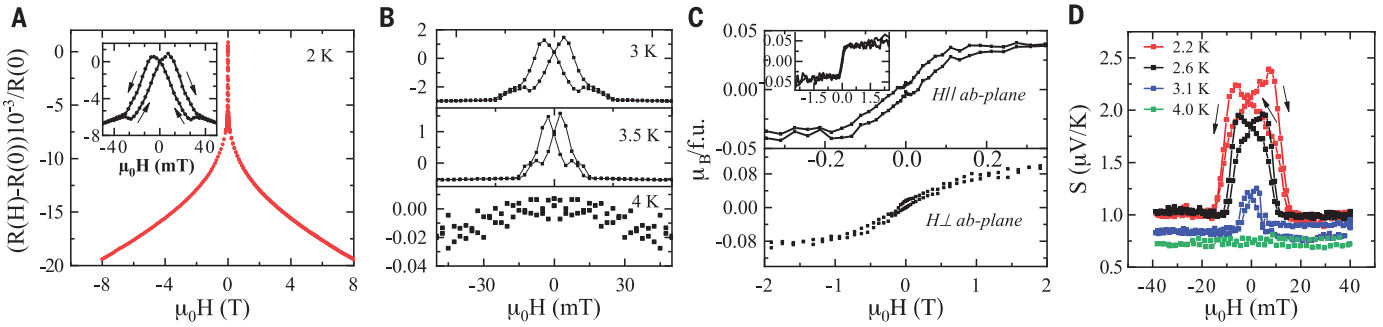

Fig. 2. Magnetotransport and magnetization for x = 0.19 in LCCO. Shown are the data for a sample on STO substrate. (**A**) *ab*-plane Δρ(%) = [ρ(*H*) − ρ(0)]/ρ(0) × 100 (*H* ⊥ *ab*-plane) at 2 K. Inset: Δρ(%) for low fields. Black arrows indicate the sweeping direction of the field. (**B**) Low-field *ab*-plane Δρ(%) (*H* ⊥ *ab*-plane) at 3 K, 3.5 K, and 4 K with the same sweeping direction as in (A) (the *y*-axis label is also the same). (**C**) Magnetization versus magnetic field with *H* || *ab*-plane and *H* ⊥ *ab*-plane at 2 K. The substrate background is removed in these plots (*22*). Inset: Magnetization in extended view for *H* || *ab*-plane. (**D**) *ab*-plane thermoelectric power with transverse sweeping field +400 Oe to −400 Oe.

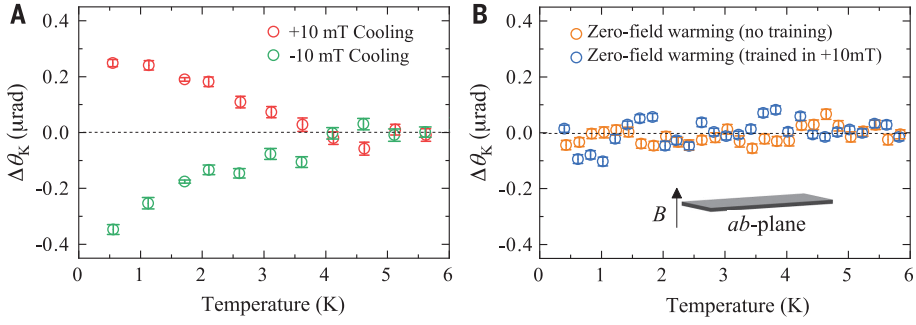

Fig. 3. Polar Kerr effect in LCCO. (**A**) Kerr angle measured in zero magnetic field after cooling down from 6 K in +10 mT (red) and −10 mT (green), plotted as a function of temperature for an LCCO sample with x = 0.19 (*H* ⊥ *ab*-plane, LSAT substrate). Data are averaged over 500-mK windows, and we subtract a temperature-independent background offset of ~0.7 μm stemming from electrical and optical contributions from the instruments. Error bars indicate SD. An onset of Kerr signal at 4 K and a complete reversal with opposite magnetic field indicate field-canted moments along the polar direction. (**B**) Kerr angle measured in zero magnetic field while warming after cooling down in zero magnetic field (orange) and after cooling down in +10 mT (blue). Data are averaged over 200 mK windows, and we subtract a temperature-independent background offset of roughly 0.7 μm. There is no discernible Kerr signal, indicating that the magnetic moments are in the *ab*-plane. Inset: Direction of the applied magnetic field for all Kerr measurements.

tiny magneto-optic effects on the order of tens of nanoradians, as described in (*23*). This technique has been used to detect time-reversal symmetry breaking in triplet superconductors (*24*, *25*) as well as the ferromagnetic phase transition of a thin film of $SrRuO_3$ (*26*). For all the Kerr measurements, we operated at a wavelength of 1550 nm with a spot size D ~ 10.6 μm and measured with an incident optical power P_{inc} ~ 30 μW. The details of these measurements are given in the Fig. 3 caption and (*22*). These results fully confirm the transport and magnetization results and indicate the onset of long-range ferromagnetic order at ~4 K. Moreover, the magnitude of the Kerr angle θ_K is consistent with the magnetic moment found from the magnetization results (*22*).

Taken together, the negative transverse magnetoresistance, anisotropic magnetoresistance, and hysteretic features in magnetoresistance, magneto-thermopower, and magnetization measurements, as well as the finite polar Kerr effect, provide compelling evidence for static ferromagnetic order below 4 K in overdoped LCCO. Great care was taken to ensure that the observed magnetism was intrinsic to the sample (*22*), including the reproduction of our results for more than 20 films grown on three different substrates. For example, magnetoresistance hysteresis similar to that shown in Figs. 1 and 2 for LCCO on an STO substrate was found for LCCO films on LSAT and $LaSrGaO_4$ substrates (fig. S3). Magnetization hysteresis of LCCO on LSAT is shown in fig. S1C; the Kerr effect was done for LCCO films on an LSAT substrate (Fig. 3).

The ferromagnetism we observe in overdoped nonsuperconducting LCCO resembles that found in weak itinerant ferromagnets such as UGe_2 (*27*) and Y_4Co_3 (*28*), in that they also exhibit a T^2 temperature dependence of the resistivity. The ferromagnetic order may exist above the doping x = 0.19, but we were unable to prepare such films. The onset of superconductivity at 5 K for x = 0.17 prohibits a lower-temperature magnetoresistance study for this and lower dopings. However, we measured an x ~ 0.175 film that might be superconducting below 1.8 K. This film shows a positive normal-state magnetoresistance at 1.8 K and no low-field hysteretic magnetoresistance (fig. S12), which means that it is not ferromagnetic at 1.8 K. On the basis of this result, the magnetoresistance data in Fig. 1, and a prior μSR study of LCCO (*29*), it is reasonable to predict the absence of any ferromagnetic order below x = 0.175. We attribute the observed ferromagnetism to the hypothesized (*15*) low-temperature ferromagnetic order in the copper oxide planes of overdoped cuprates.

A previous transport study observed quantum critical behavior of unknown origin at the end of the superconducting dome in LCCO based on the scaling of the resistivity with temperature and magnetic field. The work reported the low-temperature normal-state resistivity to vary as $T^{1.6}$ for a doping at the end of the dome (*30*). This power law of resistivity is very close to the power law expected to arise from quantum critical ferromagnetic fluctuations (*31*). In conjunction with the evidence for ferromagnetic order above the superconducting dome described in this work, these results are suggestive of a superconducting/ferromagnetic quantum critical point located at the end of the superconducting dome in LCCO.

Our study firmly establishes the existence of itinerant ferromagnetic order in the overdoped, nonsuperconducting, cuprate LCCO at temperatures below 4 K. This suggests the

presence of a ferromagnetic quantum critical point at the end of the superconducting dome, and a resultant competition between d-wave superconductivity and ferromagnetism. This competition may play a role in other unexplained aspects of the overdoped cuprates, such as the decrease of T_c beyond optimal doping and the anomalous loss of superfluid density (*32*). However, further work will be needed to learn more about the nature of the ferromagnetic phase and its impact on the properties of overdoped cuprates. Nonetheless, this striking observation of itinerant ferromagnetism may help to address the long-standing mystery of the cuprates and to reimagine the unexplored frontiers of their phase diagram. Finally, it is possible that this ferromagnetic order represents another intriguing similarity between the cuprates and twisted bilayer graphene, given that ferromagnetic order has recently been found beyond the superconducting dome in that system (*33*).

REFERENCES AND NOTES

1. P. A. Lee, N. Nagaosa, X.-G. Wen, *Rev. Mod. Phys.* **78**, 17–85 (2006).
2. B. Keimer, S. A. Kivelson, M. R. Norman, S. Uchida, J. Zaanen, *Nature* **518**, 179–186 (2015).
3. T. Wu *et al.*, *Nature* **477**, 191–194 (2011).
4. M. Hücker *et al.*, *Phys. Rev. B* **90**, 054514 (2014).
5. E. H. da Silva Neto *et al.*, *Sci. Adv.* **2**, e1600782 (2016).
6. R. Daou *et al.*, *Nature* **463**, 519–522 (2010).
7. M. R. Norman, D. Pines, C. Kallin, *Adv. Phys.* **54**, 715–733 (2005).
8. R. L. Greene, P. R. Mandal, N. R. Poniatowski, T. Sarkar, *Annu. Rev. Condens. Matter Phys.* **11**, 213–229 (2020).
9. A. Legros *et al.*, *Nat. Phys.* **15**, 142–147 (2019).
10. P. R. Mandal, T. Sarkar, R. L. Greene, *Proc. Natl. Acad. Sci. U.S.A.* **116**, 5991–5994 (2019).
11. T. Sarkar, P. R. Mandal, N. R. Poniatowski, M. K. Chan, R. L. Greene, *Sci. Adv.* **5**, eaav6753 (2019).
12. R. A. Cooper *et al.*, *Science* **323**, 603–607 (2009).
13. J. E. Sonier *et al.*, *Proc. Natl. Acad. Sci. U.S.A.* **107**, 17131–17134 (2010).
14. K. Kurashima *et al.*, *Phys. Rev. Lett.* **121**, 057002 (2018).
15. A. Kopp, A. Ghosal, S. Chakravarty, *Proc. Natl. Acad. Sci. U.S.A.* **104**, 6123–6127 (2007).
16. K. Jin, N. P. Butch, K. Kirshenbaum, J. Paglione, R. L. Greene, *Nature* **476**, 73–75 (2011).
17. J. M. D. Coey, *Magnetotransport in Magnetism and Magnetic Materials* (Cambridge Univ. Press, 2009).
18. M. Viret *et al.*, *Phys. Rev. B* **53**, 8464–8468 (1996).
19. T. R. McGuire, R. I. Potter, *IEEE Trans. Magn. Mater* **11**, 1018–1038 (1975).
20. H. Boschker *et al.*, *Phys. Rev. X* **9**, 011027 (2019).
21. Y. Pu, E. Johnston-Halperin, D. D. Awschalom, J. Shi, *Phys. Rev. Lett.* **97**, 036601 (2006).
22. See supplementary materials.
23. A. Kapitulnik, J. Xia, E. Schemm, A. Palevski, *New J. Phys.* **11**, 055060 (2009).
24. J. Xia, Y. Maeno, P. T. Beyersdorf, M. M. Fejer, A. Kapitulnik, *Phys. Rev. Lett.* **97**, 167002 (2006).
25. E. R. Schemm, W. J. Gannon, C. M. Wishne, W. P. Halperin, A. Kapitulnik, *Science* **345**, 190–193 (2014).
26. J. Xia, W. Siemons, G. Koster, M. R. Beasley, A. Kapitulnik, *Phys. Rev. B* **79**, 140407(R) (2009).
27. S. S. Saxena *et al.*, *Nature* **406**, 587–592 (2000).
28. A. Kolodziejczyk, J. Spalek, *J. Phys. F* **14**, 1277–1289 (1984).
29. H. Saadaoui *et al.*, *Nat. Commun.* **6**, 6041 (2015).
30. N. P. Butch, K. Jin, K. Kirshenbaum, R. L. Greene, J. Paglione, *Proc. Natl. Acad. Sci. U.S.A.* **109**, 8440–8444 (2012).
31. T. Moriya, K. Ueda, *Rep. Prog. Phys.* **66**, 1299–1341 (2003).
32. I. Božović, X. He, J. Wu, A. T. Bollinger, *Nature* **536**, 309–311 (2016).
33. A. L. Sharpe *et al.*, *Science* **365**, 605–608 (2019).
34. T. Sarkar *et al.*, Ferromagnetic order beyond the superconducting dome in a cuprate superconductor, Dryad (2020); https://doi.org/10.5061/dryad.05qfttf08.

ACKNOWLEDGMENTS

We thank M. Coey, J. Mannhart, J. Paglione, N. Butch, W. Fuhrman, and J. Higgins for helpful discussions and comments on the manuscript. **Funding:** The work at the University of Maryland is supported by NSF under grant DMR-1708334, AFSOR under grant FA9550-14-10332, and the Maryland Quantum Materials Center. Work at Stanford University was supported by the Department of Energy, Office of Basic Energy Sciences, under contract DE-AC02- 76SF00515. D.S.W. acknowledges support from the Karel Urbanek Postdoctoral Fellowship in Applied Physics at Stanford University. J.Z. acknowledges support from the Chinese Government Scholarship of China Scholarship Council. The Kerr effect experiments were funded in part by a QuantEmX grant from ICAM and the Gordon and Betty Moore Foundation through grant GBMF5305 to N.R.P. **Author contributions:** R.L.G. directed the overall project. A.K. directed the research at Stanford; T.S. performed the transport and magnetization measurements and analysis; P.R.M. performed the thermoelectric measurement; T.S. prepared the samples with assistance from N.R.P.; D.S.W. and J.Z. performed the Kerr effect measurements and analysis with assistance from N.R.P.; and R.L.G., T.S., N.R.P., and A.K. wrote the manuscript and discussed it with all other authors. **Competing interests:** The authors declare no competing financial interests. **Data and materials availability:** All data needed to evaluate the conclusions in the paper or the supplementary materials are available on Dryad (*34*).

SUPPLEMENTARY MATERIALS

science.sciencemag.org/content/368/6490/532/suppl/DC1
Materials and Methods
Supplementary Text
Figs. S1 to S12
References (*35*–*46*)

26 February 2019; resubmitted 23 October 2019
Accepted 25 March 2020
10.1126/science.aax1581

Science

Ferromagnetic order beyond the superconducting dome in a cuprate superconductor

Tarapada Sarkar, D. S. Wei, J. Zhang, N. R. Poniatowski, P. R. Mandal, A. Kapitulnik and Richard L. Greene

Science **368** (6490), 532-534.
DOI: 10.1126/science.aax1581

An unexpected order

The phase diagram of cuprate superconductors, in addition to superconductivity, contains many ordered states such as antiferromagnetism, charge density waves, and nematicity. Sarkar *et al.* show that ferromagnetism should be added to this list. Studying thin films of $La_{2-x}Ce_xCuO_4$ at high dopings, past the point at which superconductivity disappears, the researchers found signatures of ferromagnetism in both the transport and optical properties of the films.
Science, this issue p. 532